

# Ferromagnetism and Nematicity of Fermions in an Optical Flux Lattice

Stefan K. Baur and Nigel R. Cooper

*T.C.M. Group, Cavendish Laboratory, J. J. Thomson Avenue, Cambridge CB3 0HE, United Kingdom*

(Dated: July 19, 2022)

Ultracold atoms in Raman-dressed optical lattices allow for effective momentum-dependent interactions among single-species fermions originating from short-range s-wave interactions. These dressed-state interactions combined with very flat bands encountered in the recently introduced optical flux lattices push the Stoner instability towards weaker repulsive interactions, making it accessible with current experiments. As a consequence of the coupling between spin and orbital degrees of freedom, the magnetic phase features Ising nematic order.

PACS numbers: 67.85.Lm, 03.75.Ss, 03.65.Vf, 73.22.Gk

Recently, there has been considerable effort to observe the Stoner instability to itinerant ferromagnetism with ultracold gases [1–5]. So far, this effort has been fruitless and it has been argued that rapid dimer formation at the large coupling strength that is required for ferromagnetism precludes the formation of magnetic domains [6, 7]. Here we show that atoms subjected to optical lattices involving coherent Raman coupling of internal states can have a strongly enhanced Stoner instability. The ferromagnetic phase appears at much weaker coupling strength where the gas is less susceptible to dimer formation. Furthermore, our results display several intriguing novel phenomena, such as interaction-induced phase transitions between distinct Fermi surface topologies and nematic ordering, allowing close parallels between the physics of cold gases and phenomena in diverse systems such as high temperature superconductors, ruthenates and quantum Hall systems [8].

Central to our studies are the novel effects that arise when atoms are subjected to Raman dressing. Raman dressing has recently been used in experiments to create artificial gauge potentials [9–11] and to induce effective higher partial-wave interactions among identical bosons from short-ranged s-wave interactions [12]. We consider an atomic Fermi gas subjected to an optical flux lattice [13], in which both of these effects are important. The orbital effects of the gauge field cause the lowest energy band of the optical flux lattice to be very narrow in energy even for a shallow lattice far from the tight-binding limit. Interactions among fermionic atoms in this lowest band remain sizeable [14]. Simple s-wave interactions between distinct bare fermions give rise to effective interactions of non-zero range among single species fermions of the lowest band [14, 15]. We show that these interactions, within this narrow band, cause a ferromagnetic transition at a much smaller coupling than in the continuum. In view of the coupling of spin and orbital motion through the Raman dressing, the ferromagnetic transition appears as a change in Fermi surface topology. Furthermore, it is accompanied by a reduction of the (spatial) crystal symmetry so also involves nematic order [8]. As we describe, this coupling of spin and or-

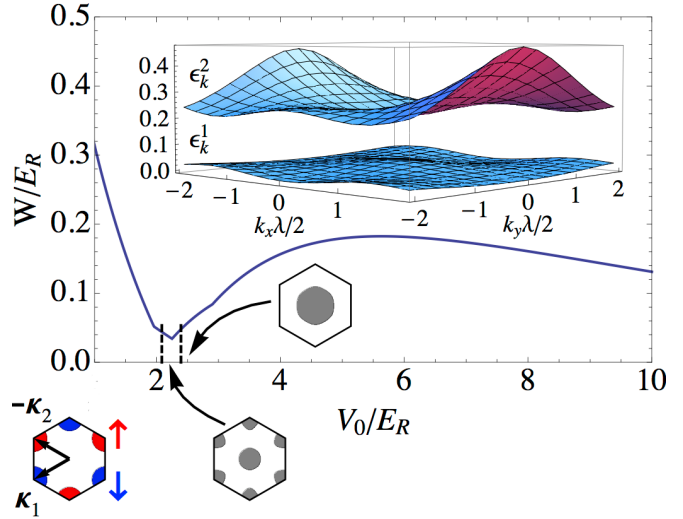


FIG. 1: (Color online) Bandwidth  $W$  of the lowest band as a function of lattice depth of the optical flux lattice discussed in the main text (with  $\theta = 0.3$  and  $\epsilon = 0.4$ ). The inset shows the dispersion of the lowest two bands for  $V_0/E_R = 2.25$ . As the lattice is ramped up, the dispersion of the lowest band develops a minimum at the center of the Brillouin zone causing reconstruction of the Fermi surface for non-interacting particles. The locations where these reconstructions occur for filling  $\nu = 1/4$  are marked by the dashed lines. For vanishing lattice depth  $V_0 = 0$  the Fermi circles of the spin- $\uparrow$  (red) and spin- $\downarrow$  (blue) are displaced from each other to the corners of the Brillouin zone.

bital motion allows the magnetic/nematic ordering to be readily measured in experiment by band-mapping techniques.

We consider the implementation of an optical flux lattice of Ref. [14], which involves two-photon dressing of hyperfine states. We focus on an atomic species with groundstate angular momentum  $F = 1/2$ , but our key ideas are readily extended to atoms with larger  $F$  as described at the end of the paper. We further restrict attention to a quasi-2D geometry, assuming an in-plane confinement energy that is large compared to all other energy scales.

The optical flux lattice is formed by interference of three linearly polarized in-plane laser beams with wave vectors  $\kappa_1 = -\kappa/2(\sqrt{3}, 1)$ ,  $\kappa_2 = \kappa/2(\sqrt{3}, -1)$  and  $\kappa_3 = \kappa(0, 1)$ . A fourth circular polarized laser beam, oriented perpendicular to the 2D plane, provides the other frequency required for two-photon Raman coupling of the Zeeman-split hyperfine states.

This optical potential leads to a single particle Hamiltonian

$$\hat{H}_0 = \frac{\mathbf{p}^2}{2m} \hat{\mathbb{1}} + V_{\text{sc}}(\mathbf{r}) \hat{\mathbb{1}} + \hat{\boldsymbol{\sigma}} \cdot \mathbf{B}(\mathbf{r}), \quad (1)$$

in which the atom experiences a scalar potential

$$V_{\text{sc}} = V_0(3 \cos^2(\theta) - 1) \sum_j \cos(\kappa'_j \cdot \mathbf{r}) \quad (2)$$

and its spin  $\hat{\boldsymbol{\sigma}}$  couples to an effective magnetic field

$$B_z = \sqrt{3} V_0 \sin^2(\theta) \sum_j \sin(\kappa'_j \cdot \mathbf{r}) \quad (3)$$

$$B_x + iB_y = \epsilon V_0 \cos(\theta) \sum_j e^{-i\kappa_j \cdot \mathbf{r}}. \quad (4)$$

$V_0$  denotes the lattice depth,  $\theta$  is the polarization angle of the in-plane beams with respect to the surface normal,  $\epsilon$  is proportional to the ratio between Raman coupling and scalar potential, and  $\kappa'_1 = \kappa_1 - \kappa_2$ ,  $\kappa'_2 = \kappa_3 - \kappa_1$  and  $\kappa'_3 = \kappa_2 - \kappa_3$  [14]. The geometry of the Raman beams is such that conversion from spin- $\uparrow$  to spin- $\downarrow$  involves a momentum exchange of  $\kappa_1$ ,  $\kappa_2$  or  $\kappa_3$ . This causes the spin character of the Bloch states to vary with crystal momentum within the Brillouin zone. (The reciprocal lattice basis vectors can be taken to be  $\mathbf{G}_1 \equiv \kappa_1 - \kappa_3$  and  $\mathbf{G}_2 \equiv \kappa_2 - \kappa_3$ .) Notably, for vanishing lattice depth  $V_0 = 0$ , when the energy eigenstates are simply plane waves for spin- $\uparrow$  and spin- $\downarrow$ , the crystal momentum for the spin- $\downarrow$  ( $\uparrow$ ) state with zero kinetic energy is simply  $\kappa_1$  ( $-\kappa_2$ ), or any equivalent point related by the addition of reciprocal lattice vectors. Hence, the crystal momenta of the two spin states are displaced from each other within the Brillouin zone. In this limit  $V_0 = 0$ , an unpolarized state of non-interacting fermions therefore appears as two filled Fermi circles, centered on  $\kappa_1$  ( $-\kappa_2$ ) for spin- $\downarrow$  ( $\uparrow$ ) and shown in blue (red) in Fig. 1.

The width of the lowest-energy band is shown in Fig. 1 as a function of the overall lattice depth  $V_0$  for fixed values of  $\epsilon$  and  $\theta$ . The bandwidth passes through a minimum at  $V_0/E_R \simeq 2$ , with the recoil energy defined by  $E_R \equiv \hbar^2 \kappa^2 / (2m)$ . This is the regime where the optical flux lattice best mimics the orbital effects of a uniform magnetic field. The lowest energy band is similar to a Landau level: with small bandwidth and Chern number of one [14]. In the vicinity of this point the positions of the band minima change within the Brillouin zone. (Similar features are found in tight-binding models of Chern

insulators when next nearest-neighbor hoppings are included [16].) This reconstruction is illustrated in Fig. 1 by the non-interacting Fermi surfaces shown for a band filling of  $\nu = 1/4$ . Note that at  $V_0 = 0$  the Fermi surface consists of two disconnected circles: these are the spin-up and spin-down Fermi surfaces, displaced in crystal momentum as described above.

For non-zero  $V_0/E_R$  the spin composition of the Bloch state continuously varies with crystal momentum. As a result,  $s$ -wave interactions between spin-up and spin-down components lead to effective momentum-dependent interactions between fermions in this band. It is remarkable that even though we started with a model of short-ranged interactions, we obtain an effective theory of interacting spin-less fermions [14].

Atoms restricted to states in the lowest band are described by the effective Hamiltonian

$$H_{lb} = \sum_{\mathbf{k}} \epsilon_{\mathbf{k}} c_{\mathbf{k}}^\dagger c_{\mathbf{k}} + \frac{1}{2} \sum_{\mathbf{k}_1 \mathbf{k}_2 \mathbf{k}_3 \mathbf{k}_4} V_{\mathbf{k}_1 \mathbf{k}_2 \mathbf{k}_3 \mathbf{k}_4} c_{\mathbf{k}_1}^\dagger c_{\mathbf{k}_2}^\dagger c_{\mathbf{k}_3} c_{\mathbf{k}_4} \quad (5)$$

where  $\epsilon_{\mathbf{k}}$  is the band dispersion,  $c_{\mathbf{k}}^{(\dagger)}$  are the fermionic field operators for state of crystal momentum  $\mathbf{k}$ , and

$$V_{\mathbf{k}_1 \mathbf{k}_2 \mathbf{k}_3 \mathbf{k}_4} = g_{2D} \int d^2 \mathbf{r} \sum_{\sigma} \phi_{\mathbf{k}_1 \sigma}^*(\mathbf{r}) \phi_{\mathbf{k}_2 \bar{\sigma}}^*(\mathbf{r}) \phi_{\mathbf{k}_3 \bar{\sigma}}(\mathbf{r}) \phi_{\mathbf{k}_4 \sigma}(\mathbf{r})$$

is the effective interaction in the lowest band in terms of the eigenfunctions  $(\phi_{\mathbf{k}\uparrow}(\mathbf{r}), \phi_{\mathbf{k}\downarrow}(\mathbf{r}))^T$  of the single particle Hamiltonian (1). In the following we characterize the bare interaction strength by the dimensionless coupling parameter  $\tilde{g} \equiv mg_{2D}/\hbar^2$ .

To study the effects of interactions, we perform a Hartree-Fock (HF) variational approximation which results in the energy functional

$$E[n_{\mathbf{k}}] = \sum_{\mathbf{k}} \epsilon_{\mathbf{k}} n_{\mathbf{k}} + \frac{1}{2} \sum_{\mathbf{k}\mathbf{k}'} V_{\mathbf{k}\mathbf{k}'} n_{\mathbf{k}} n_{\mathbf{k}'} \quad (6)$$

with  $V_{\mathbf{k}\mathbf{k}'} = V_{\mathbf{k}\mathbf{k}'\mathbf{k}'\mathbf{k}'} - V_{\mathbf{k}\mathbf{k}'\mathbf{k}'\mathbf{k}'}$ . For our zero-temperature results, we find the ground states that minimize Eq. (6) for a fixed total number of particles  $N = \sum_{\mathbf{k}} n_{\mathbf{k}}$ . This is achieved by setting the occupation numbers  $n_{\mathbf{k}}$  equal to unity for the  $N$  orbitals with lowest HF energies

$$\xi_{\mathbf{k}} = \epsilon_{\mathbf{k}} + \sum_{\mathbf{k}'} V_{\mathbf{k}\mathbf{k}'} n_{\mathbf{k}'}. \quad (7)$$

We determine these energies self-consistently by numerical iteration, discretizing momenta of the Brillouin zone on a fine grid [17]. For our results at non-zero temperature  $T$ , we instead find  $n_{\mathbf{k}}$  by minimizing the thermodynamic potential  $\Omega = E - TS - \mu N$  where  $\mu$  is the chemical potential and  $S = -k_B \sum_{\mathbf{k}} n_{\mathbf{k}} \ln(n_{\mathbf{k}}) + (1 - n_{\mathbf{k}}) \ln(1 - n_{\mathbf{k}})$  is the entropy. The grand canonical potential is stationary ( $\delta\Omega/\delta n_{\mathbf{k}} = 0$ ) when

$$n_{\mathbf{k}} = \frac{1}{e^{(\xi_{\mathbf{k}} - \mu)/k_B T} + 1} \quad (8)$$

which we numerically iterate to self-consistency with Eq. (7). We start from different trial states and then compare their grand canonical potentials in order to find the minimum free energy configuration.

Our results show a robust ferromagnetic phase for a wide range of parameters. To characterize this phase we use the magnetization per particle along the  $z$ -direction as an order parameter

$$m_z = \frac{1}{\nu} \int_{A_{\text{cell}}} d^2r [n_{\uparrow}(\mathbf{r}) - n_{\downarrow}(\mathbf{r})]. \quad (9)$$

In Fig. 2 we show the (modulus of the) calculated order parameter at zero temperature for a band filling of  $\nu = 1/4$ , as a function of 2D coupling  $\tilde{g}$  and of lattice depth  $V_0/E_R$ . These results are representative of other fillings with  $\nu \lesssim 1/2$ . In the absence of any lattice,  $V_0/E_R = 0$ , there is a transition from paramagnet to ferromagnet at  $\tilde{g}_c = 2\pi$ . This is the conventional Stoner instability for fermions with contact repulsion in 2D [18]. This transition appears as a reconstruction of the Fermi surface from two Fermi circles to one Fermi circle. As the lattice depth is increased, our results show a steady decrease of the coupling at which the ferromagnetic transition occurs. The minimum coupling for ferromagnetism arises for  $V_0/E_R \simeq 2$ , close to the condition for minimum bandwidth, Fig. 1. We find that the interaction strength  $\tilde{g}_c$  required is reduced from its free-space value by a factor of about 1/4. This is one of the main results of this paper: the reduction of coupling as compared to the free-space case means that ferromagnetism can be achieved without requiring as close an approach to a Feshbach resonance. A change of coupling by a factor of 1/4 is expected to have a very dramatic reduction in the rate of dimer formation [19–21].

In addition to transitions between distinct Fermi surface topologies, phases of interacting fermions can also spontaneously break lattice symmetries. For our model, we find that the appearance of ferromagnetism, with non-zero magnetization, is also accompanied by a breaking of rotational symmetry. We argue that this is a general feature of Raman-dressed atomic systems. While spin-rotational invariance is explicitly broken by the coupling of spin and orbital degrees of freedom, the optical flux lattice retains a discrete symmetry. It is invariant under a spin-flip combined with a  $2\pi/6$  rotation in real space

$$\hat{U}_6 = \hat{\sigma}_x \hat{R}_{2\pi/6}. \quad (10)$$

The Stoner ferromagnetic transition (effectively a Pomeranchuk instability in the spin-channel) causes spontaneous symmetry breaking of the  $C_6$  spin-rotation symmetry arising from  $\hat{U}_6$  down to a residual  $C_3$  symmetry associated with  $\hat{U}_6^2 = \hat{R}_{2\pi/3}$ . This phase transition is analogous to the lattice symmetry breaking in the electronic Ising nematic phases in solid state materials [8, 22–24]. Since the order parameter of the symmetry

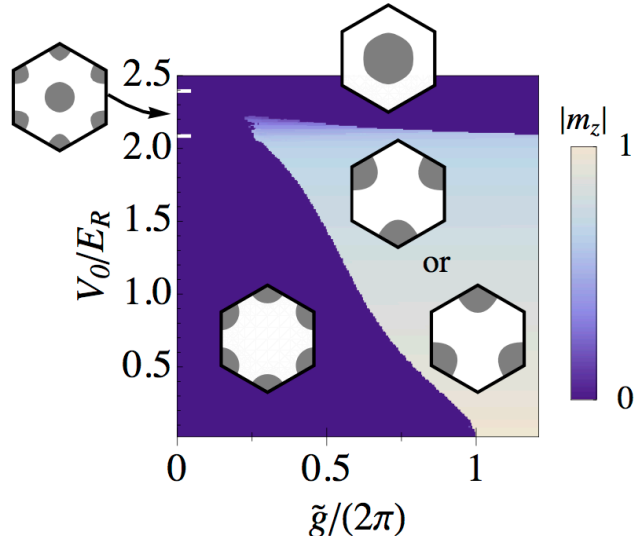


FIG. 2: (Color online) Magnetization of the ground state of interacting fermions in the lowest band of the optical flux lattice at uniform filling factor  $\nu = 1/4$  as a function of lattice depth  $V_0/E_R$  and dimensionless coupling strength  $\tilde{g}$ . The gray shaded areas on the insets illustrate occupied states in the first Brillouin zone. White lines mark transitions between unmagnetized states of different Fermi surface topology.

broken phase is in the 2D Ising universality class, we expect this phase to survive to non-zero temperature.

The phase diagram at non-zero temperature is shown in Fig. 3 as a function of chemical potential for a band with  $V_0/E_R = 2$  and  $\tilde{g} = 1.9$ . This shows that the ferromagnetic phase is a robust phase across a range of densities and temperatures. The maximum transition temperature of  $k_B T \simeq 0.14W$  at  $\mu - \epsilon_{\min} \simeq 1.54W$  corresponds to an entropy per particle of  $S/N \simeq 1.1$ . Entropies of this order are being reached in current optical lattice experiments [25].

At the lowest temperatures, we find evidence for the appearance of competing phases involving small scale reconstructions of the shape(s) of the individual Fermi surface(s) which can be viewed as Pomeranchuk instabilities. We do not pursue these here, as we expect these low temperature phases to compete with strongly correlated phases, related to fractional quantum Hall states (at specific fillings), which cannot be accessed in HF theory, but which can commonly co-exist with ferromagnetism [28–30]. While our mean-field theory neglects correlations [26] which can lead to quantitative changes in the location of the Stoner instability, detailed numerical studies of related models show a robust ferromagnetic phase [4, 5, 27]. We expect the reduction of the critical coupling strength that we predict to be a robust feature, since the shallow optical flux lattice leads to a significant reduction in the bandwidth with small decrease in the interaction matrix elements.

Experimental studies of the ferromagnetic transition

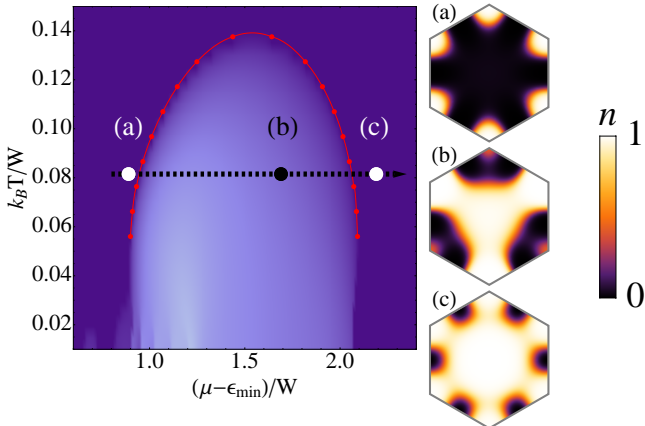


FIG. 3: (Color online) Left: Magnetization for  $V_0/E_R = 2$ ,  $\theta = 0.3$ ,  $\epsilon = 0.4$  and  $\tilde{g} = 1.9$  as a function of temperature and chemical potential (scale same for  $m_z$  as in Fig. 2).  $W$  is the bandwidth, and  $\mu - \epsilon_{\min}$  is the chemical potential measured from the bottom of the lowest band. The red dots lie on the spinodal where the symmetric state becomes unstable (the line is a guide to the eye). Right: Occupation numbers  $n_{\mathbf{k}}$  within the first Brillouin-zone for  $(\mu - \epsilon_{\min})/W = 0.89$ ,  $1.69$ ,  $2.19$  corresponding to (a), (b), (c).

we predict will require the use of an atomic species for which both strong interactions and Raman coupling can be achieved without significant heating. For a hyperfine groundstate of  $F = 1/2$ , the natural candidates are  $^{171}\text{Yb}$  or  $^{199}\text{Hg}$  [14]. For  $^{171}\text{Yb}$ , s-wave contact interactions between the two states of the lowest hyperfine manifold (as spin- $\uparrow/\downarrow$ ) can be conveniently tuned via an optical Feshbach resonance [31, 32]. Another possibility is to use an effective two-level system formed by exploiting the quadratic Zeeman effect to Raman couple two of the hyperfine states in the  $F = 9/2$  groundstate manifold of  $^{40}\text{K}$  with neighboring  $m_F$  [10]. The interstate interactions can be conveniently tuned by one of the set of magnetic Feshbach resonances that exist for these levels.

The most direct way to measure the order parameter, in Figs. 2 and 3, is by individually imaging the total spin populations  $N_{\uparrow,\downarrow}$ . An important practical consequence of the coupling of spin and orbital degrees of freedom is that total magnetization is not conserved. Hence this allows the formation of a macroscopic net magnetization starting from an initially unpolarized gas. Measurements of the net magnetization will give the average properties of the inhomogeneous cloud in the trap. If in addition one can measure the local in-situ spin populations  $n_{\uparrow,\downarrow}(\mathbf{r})$  along a contour of fixed filling factor one could then map out the phase diagram at different fillings and lattice depth analogous to recent studies of two-dimensional Bose gases [33].

Another complementary probe sensitive to the (trap averaged) Fermi surface of the dressed lowest band fermions is the adiabatic band mapping technique [34,

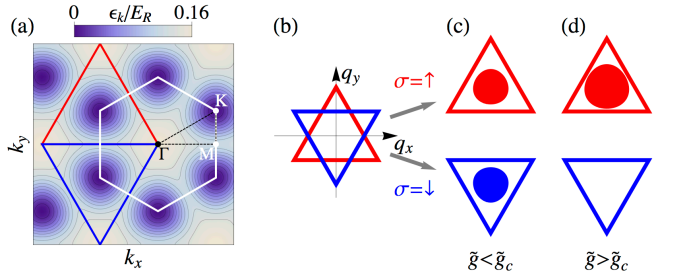


FIG. 4: (Color online) Experimental signatures of adiabatic band mapping. (a) Contour plot of the dispersion  $\epsilon_{\mathbf{k}}$  for  $V_0/E_R = 1.8$ , indicating a rhombus shaped reciprocal lattice unit cell. The Bloch states inside the upper red (lower blue) triangle in (a) map to spin- $\uparrow$  ( $\downarrow$ ) states with free space momentum  $\mathbf{q}$  illustrated in (b). For a completely filled lowest band one would observe a fully occupied hexagram (b). When the atoms pass subsequently through a Stern-Gerlach filter, the two spin states can be separately resolved. This would allow clear signatures of the transition from (c) unmagnetized to (d) magnetized phase.

35]. This probe has the additional advantage that it also allows the detection of unmagnetized phases with different Fermi surface topologies. Here the lattice potential is ramped down at a rate slow compared to the band gap and fast compared to many-particle dynamics. Then the Raman-dressed Bloch states are adiabatically mapped onto free-particle plane-wave states of definite spin, which can be imaged after time-of-flight expansion.

The form of this mapping can be deduced by recalling that for vanishing lattice depth,  $V_0 = 0$ , the spin- $\downarrow$  ( $\uparrow$ ) free-particle state with zero kinetic energy has crystal momentum  $\boldsymbol{\kappa}_1$  ( $-\boldsymbol{\kappa}_2$ ) (or any point related by reciprocal lattice vectors). Under adiabatic band-mapping, a Bloch state whose crystal momentum  $\mathbf{k}$  is closer to  $\boldsymbol{\kappa}_1$  than to  $-\boldsymbol{\kappa}_2$  is mapped to the spin- $\downarrow$  state with free-space momentum  $\mathbf{q} = \mathbf{k} - \boldsymbol{\kappa}_1$ ; if  $\mathbf{k}$  is closer to  $-\boldsymbol{\kappa}_2$  the Bloch state is mapped to the spin- $\uparrow$  state with free-space momentum  $\mathbf{q} = \mathbf{k} + \boldsymbol{\kappa}_2$ . This construction is illustrated in Fig. 4.

For a completely filled lowest band the occupied states appear then as a hexagram (superimposed triangles for spin  $\uparrow$  and  $\downarrow$ ) after band mapping as shown in Fig. 4(b). A spin resolved image of the cloud of atoms after band mapping, obtained either by appropriate detuning of imaging lasers or a Stern-Gerlach filter, allows therefore for reconstruction of the occupation numbers  $n_{\mathbf{k}}$ . Finally, we note that signatures of the change in Fermi surface topology will also appear in the Hall response [36], since the Berry curvature of the lowest band of the optical flux lattice is non-uniform [37], so the Hall coefficient is sensitive to the distribution  $n_{\mathbf{k}}$ .

We thank Z. Hadzibabic, M. Fischer, G. Conduit and J. Levinsen for useful discussions. The work has been supported by EPSRC Grants EP/I010580/1 and EP/F032773/1.

---

[1] R. A. Duine and A. H. MacDonald, Phys. Rev. Lett. **95**, 230403 (2005).

[2] G. J. Conduit and B. D. Simons, Phys. Rev. Lett. **103**, 200403 (2009).

[3] G.-B. Jo *et al.*, Science **325**, 1521 (2009).

[4] S. Pilati, G. Bertaina, S. Giorgini, and M. Troyer, Phys. Rev. Lett. **105**, 030405 (2010).

[5] S.-Y. Chang, M. Randeria, and N. Trivedi, Proc. Natl. Acad. Sci. **108**, 51 (2011).

[6] D. Pekker *et al.*, Phys. Rev. Lett. **106**, 050402 (2011).

[7] C. Sanner *et al.*, Phys. Rev. Lett. **108**, 240404 (2012).

[8] E. Fradkin *et al.*, Annu. Rev. Cond. Mat. **1**, 153 (2010).

[9] Y. J. Lin *et al.*, Nature **462**, 628 (2009).

[10] P. Wang *et al.*, Phys. Rev. Lett. **109**, 095301 (2012).

[11] L. W. Cheuk *et al.*, Phys. Rev. Lett. **109**, 095302 (2012).

[12] R. A. Williams *et al.*, Science **335**, 314 (2012).

[13] N. R. Cooper, Phys. Rev. Lett. **106**, 175301 (2011).

[14] N. R. Cooper and J. Dalibard, Europhys. Lett. **95**, 66004 (2011).

[15] X. Cui, Phys. Rev. A **85**, 022705 (2012).

[16] E. Tang, J.-W. Mei, and X.-G. Wen, Phys. Rev. Lett. **106**, 236802 (2011).

[17] We discretize momentum space with up to  $54 \times 54$  grid points, which is sufficient to remove any finite size effects from the results presented.

[18] G. J. Conduit, Phys. Rev. A **82**, 043604 (2010).

[19] D. S. Petrov, Phys. Rev. A **67**, 010703 (2003).

[20] C. Sanner *et al.*, Phys. Rev. Lett. **108**, 240404 (2012).

[21] L. Pricoupenko and M. Olshanii, J. Phys. B **40**, 2065 (2007).

[22] H. Yamase and H. Kohno, J. Phys. Soc. Jpn. **69**, 332 (2000); **69**, 2151 (2000).

[23] C. J. Halboth and W. Metzner, Phys. Rev. Lett. **85**, 5162 (2000).

[24] H. Yamase, V. Oganesyan, and W. Metzner, Phys. Rev. B **72**, 035114 (2005).

[25] R. Jördens *et al.*, Phys. Rev. Lett. **104**, 180401 (2010).

[26] H. Zhai, Phys. Rev. A **80**, 051605 (R) (2009).

[27] P. N. Ma, S. Pilati, M. Troyer, and X. Dai, Nature Phys. **8**, 601 (2012).

[28] *Perspectives in Quantum Hall Effects: Novel Quantum Liquids in Low-Dimensional Semiconductor Structures*, edited by S. Das Sarma and A. Pinczuk (Wiley, New York, 1997).

[29] Y. Saiga and M. Oshikawa, Phys. Rev. Lett. **96**, 036406 (2006).

[30] H. Katsura *et al.*, Europhys. Lett. **91**, 57007 (2010).

[31] R. Ciuryło, E. Tiesinga, and P. S. Julienne, Phys. Rev. A **71**, 030701 (2005).

[32] K. Enomoto, K. Kasa, M. Kitagawa, and Y. Takahashi, Phys. Rev. Lett. **101**, 203201 (2008).

[33] C.-L. Hung, X. Zhang, N. Gemelke, and C. Chin, Nature **470**, 236 (2011).

[34] M. Greiner *et al.*, Phys. Rev. Lett. **87**, 160405 (2001).

[35] M. Köhl *et al.*, Phys. Rev. Lett. **94**, 080403 (2005).

[36] L. J. LeBlanc *et al.*, Proc. Natl. Acad. Sci. **109**, 10811 (2012).

[37] H. M. Price and N. R. Cooper, Phys. Rev. A **85**, 033620 (2012).